Dynamic influence of Rhein lysinate on HeLa cells

JIANG LIU[1,2], YONG-ZHAN ZHEN[3], JU CUI[1], GANG HU[1], JIE WEI[1], RONG XU[1], PING TU[2] and YA-JUN LIN[1]

[1]The MOH Key Laboratory of Geriatrics, Beijing Hospital, National Center of Gerontology, Beijing 100730;
[2]Department of Endocrinology, The Third Hospital of Nanchang City, Nanchang, Jiangxi 330009;
[3]Hebei Key Laboratory for Chronic Diseases, Tangshan Key Laboratory for Preclinical and Basic Research on Chronic Diseases, School of Basic Medical Sciences, North China University of Science and Technology, Tangshan, Hebei 063000, P.R. China

Received May 3, 2018; Accepted August 7, 2018

DOI: 10.3892/ijo.2018.4554

Abstract. In a previous study, it was demonstrated that Rhein lysinate (RHL) inhibited HeLa cell proliferation via a specific mechanism. The aim of the present study was to clarify the mechanism of RHL by investigating its effect on mitochondrial damage and cell apoptosis. The results indicated that RHL inhibited cell growth and proliferation in HeLa cells. HeLa cells treated with RHL developed extensive vacuolization in a dose- and time-dependent manner. Ultrastructure analysis using transmission electron microscopy revealed that the vacuoles observed were damaged mitochondria and endoplasmic reticulum. The effects of RHL on mitochondria were further confirmed by a decrease in mitochondrial membrane potential and increased generation of reactive oxygen species. The mitochondrial proteome was analyzed, and the results demonstrated that the expression of the cytoskeletal protein keratin and dermal papilla derived protein 12 (associated with the oxidation-reduction process), which are associated with mitochondrial structure and function, were decreased compared with the untreated control group. Hoechst staining, flow cytometry and western blotting also revealed that apoptosis was induced at 24 h following RHL treatment. These results confirm that RHL toxicity in HeLa cells is a dynamic process. Vacuolar degeneration appeared in HeLa cells treated with 160 μmol/l RHL during the first 6 h and with the extension of RHL treatment, cell apoptosis was presented at ~24 h in HeLa cells.

Introduction

Cervical carcinoma has a high incidence worldwide, with ~500,000 women developing the disease each year. The majority of cases occur in less developed countries where no effective screening systems are available (1). Although surgery and chemoradiotherapy are effective treatment for 80-95% of patients with early stage cancer, recurrence and metastasis remain a major cause of cancer-associated mortality (2). The incidence of cervical cancer is increasing, thus resulting in a need to develop novel effective drugs to treat this disease (3).

Traditional Chinese medicine has been used to treat a variety of illnesses for thousands of years. Rhubarb has been widely used to treat intestinal dysmotility (4) and acute renal failure (5), and has been reported to inhibit inflammatory and oxidative stresses (6) as well as tumor cell proliferation (7). Rhein, a bioactive component of rhubarb, has been demonstrated to have a number of antitumor effects, including inhibiting ERK phosphorylation, inducing G0/G1 arrest and triggering apoptosis (8-11). Rhein lysinate (RHL) is a novel compound obtained by modifying Rhein. The carboxyl group of Rhein reacts with amino-group of lysine to form RHL salt and its structure was presented in our previously published study (12). Compared with Rhein, RHL is easy to dissolve in water; however, does not affect the function of Rhein. RHL has been extensively studied for its anticancer properties (13-15). Our group previously demonstrated that RHL inhibited HeLa cell proliferation via a specific mechanism (14). In order to clarify the mechanism of RHL in HeLa cells, its effects on vacuolar degeneration and apoptosis were investigated.

Materials and methods

Materials. Rhein was purchased from Nanjing Qingze Medical Technology Development Co., Ltd. (Nanjing, Jiangsu, China). Lysine was purchased from Beijing Solarbio Science & Technology Co., Ltd. (Beijing, China). Rhein lysinate (RHL) was prepared in the MOH Key Laboratory of Geriatrics, Beijing Hospital (Beijing, China) with a purity of 98% detected by colorimetric method. Vitamin C, 2,7-dichlorfluorescein-diacetate (DCFH-DA), 3-(4,5-dimethylthiazol-2-yl)-2,5-diphenyl-tetrazolium bromide (MTT), N-acetyl cysteine (NAC), diphenylene iodonium (DPI), Rhodamine 123 and Hoechst 33342 were purchased from Merck KGaA (Sigma-Aldrich, Darmstadt, Germany). An Annexin V/propidium iodide (PI) kit was obtained from Thermo Fisher Scientific, Inc. (Waltham, MA,

Correspondence to: Professor Yajun Lin, The MOH Key Laboratory of Geriatrics, Beijing Hospital, National Center of Gerontology, Room 1010, Science and Education Building, 1 Dahua Road, Dongcheng, Beijing 100730, P.R. China
E-mail: linyajun2000@126.com

Key words: Rhein lysinate, mitochondria, vacuolar degeneration, reactive oxygen species, apoptosis

USA). Primary antibodies directed against B-cell lymphoma 2 (Bcl-2; cat. no. 15071; 1:1,000), Bcl-2-associated X protein (Bax; cat. no. 2774; 1:1,000), caspase-3 (cat. no. 9662; 1:1,000) and cleaved-caspase-3 (cat. no. 9661; 1:1,000) were purchased from Cell Signaling Technology, Inc. (Danvers, MA, USA). The primary antibody against β-actin (cat. no. sc-70319; 1:2,000) and rabbit (cat. no. sc-2004; 1:5,000) or mouse (cat. no. sc-2005; 1:5,000) IgG secondary antibodies were purchased from Santa Cruz Biotechnology, Inc. (Dallas, TX, USA). Prestained Protein marker p7708V was purchased from New England BioLabs, Inc. (Ipswich, MA, USA). Western Blot Luminol reagent and polyvinylidene difluoride (PVDF) membranes were purchased from EMD Millipore (Billerica, MA, USA).

Determination of cell proliferation. Cell proliferation was examined using an MTT assay, according to the manufacturer's protocol. HeLa cells were obtained from the American Type Culture Collection (Manassas, VA, USA) and were cultured in Dulbecco's modified Eagle's medium (DMEM; Gibco, Thermo Fisher Scientific, Inc.) supplemented with 10% fetal bovine serum (FBS), 100 μg/ml of streptomycin and 100 U/ml of penicillin at 37˚C with 5% CO_2. HeLa cells were plated onto 96-well plates ($4x10^3$ cells/well) for 24 h. Subsequently, the cells were treated with RHL (0, 20, 40, 80, 160 or 320 μmol/l) for 48 h. All assays were performed in triplicate.

Live cell imaging. HeLa cells treated with RHL 160 μmol/l were used for live cell imaging for 24 h by placing the culture dishes onto a sample stage within a heated chamber (37˚C). Live imaging was performed using an ImageXpress Micro XLS Widefield High-Content Analysis system (Molecular Devices, LLC, Sunnyvale, CA, USA). Images were captured at 40x with 10 msec exposure times in 5 min intervals using an MRm CCD camera (Carl Zeiss AG, Oberkochen, Germany), and different Z sections were projected using the softWoRx® Suite (version 2.0; Applied Precision, Inc., Mississauga, ON, Canada).

Transmission electron microscopy. To clarify whether the development of vesicles in RHL-treated HeLa cells was due to autophagy, ultrastructural analysis was performed as previously described (16). Briefly, HeLa cells were treated with 160 μmol/l RHL for 24 h, harvested and washed twice with PBS. After being fixed with ice-cold glutaraldehyde (3% in 0.1 M cacodylate buffer, pH 7.4) at 4˚C for 30 min, the samples were post-fixed with 1% OsO_4 in the same buffer at 4˚C for 1 h and subjected to electron microscopic analysis. Representative areas were chosen for ultra thin sectioning and were observed at 500kX with a 200CX transmission electron microscope (JEOL Ltd., Tokyo, Japan).

Intracellular reactive oxygen species (ROS) generation. The generation of intracellular ROS was assessed using DCFH-DA staining. HeLa cells were cultured in 6-well plates for determination of intracellular ROS generation. The cells were treated with RHL for 24 h and then stained with 10 μmol/l DCFH-DA at 37˚C for 30 min according to the manufacturer's protocol. Following staining, cells were washed with PBS. DCF fluorescence data were acquired at x20 or x10 using an inverted fluorescence microscope (Olympus Corporation, Tokyo, Japan). Fluorescence intensity was detected by ImageJ software [version 1.0; National Institutes of Health (NIH), Bethesda, MD, USA].

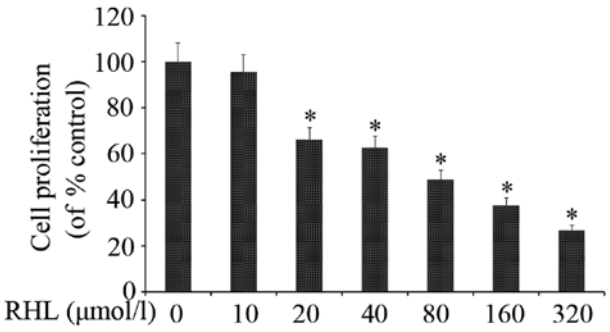

Figure 1. Effect of RHL on cell proliferation of HeLa cells. Cells were treated with various concentrations of RHL at 37˚C for 48 h. The effects on cell proliferation were examined by MTT assay, and cell proliferation was calculated as the percentage of control. All assays were done in triplicate. *P<0.05, compared with untreated control group. RHL, Rhein lysinate; MTT, 3-(4,5-dimethylthiazol-2-yl)-2,5- diphenyl-tetrazolium bromide.

Detection of the mitochondrial membrane potential (MMP) by Rhodamine 123 stain. HeLa cells were seeded in 6-well plates overnight and subsequently treated with 80 or 160 μmol/l RHL at 24-h intervals. Cells were then fixed with 4% paraformaldehyde at room temperature for 20 min. PBS was used as a negative control. Rhodamine 123 was added to cells at a final concentration of 5 μg/ml and incubated at 37˚C for 30 min to stain the mitochondria. Images were captured using an inverted fluorescence microscope (magnification, x20). Fluorescence intensity was detected by ImageJ software (version 1.0; NIH).

Mitochondrial isolation and proteomics assay. Mitochondria were isolated using a Mitochondrial Extraction kit (cat. no. SM0020) according to the manufacturer's protocol (Beijing Solarbio Science & Technology Co., Ltd.). Protein was extracted from the mitochondria and a proteomics assay was performed using label-free quantitative proteomics technology (Fanxing Boao Ltd., Beijing, China). The procedure included protein quantification, protein reduction alkylation, trypsin hydrolysis, liquid chromatography-tandem mass spectrometry (LC-MS/MS) assay and data analysis as previously described (17).

Hoechst staining fluorescence microscopy and Annexin V/PI flow cytometry. HeLa cells were seeded in a 25 cm^2 flask overnight. Cells were treated with 160 μmol/l RHL for 24, 48 or 72 h and fixed with 4% paraformaldehyde at room temperature for 20 min. PBS was used as a negative control. Hoechst was added to cells at a final concentration of 5 μg/ml and incubated at 37˚C for 30 min for nuclear staining. Images were captured using an inverted fluorescence microscope (magnification, x20). To assess cell apoptosis, treated cells were collected and stained with Annexin V and PI at room temperature for 30 min and subjected to flow cytometry with FACSCalibur and Cell Quest software (version 5.1; BD Biosciences, Franklin Lakes, NJ, USA).

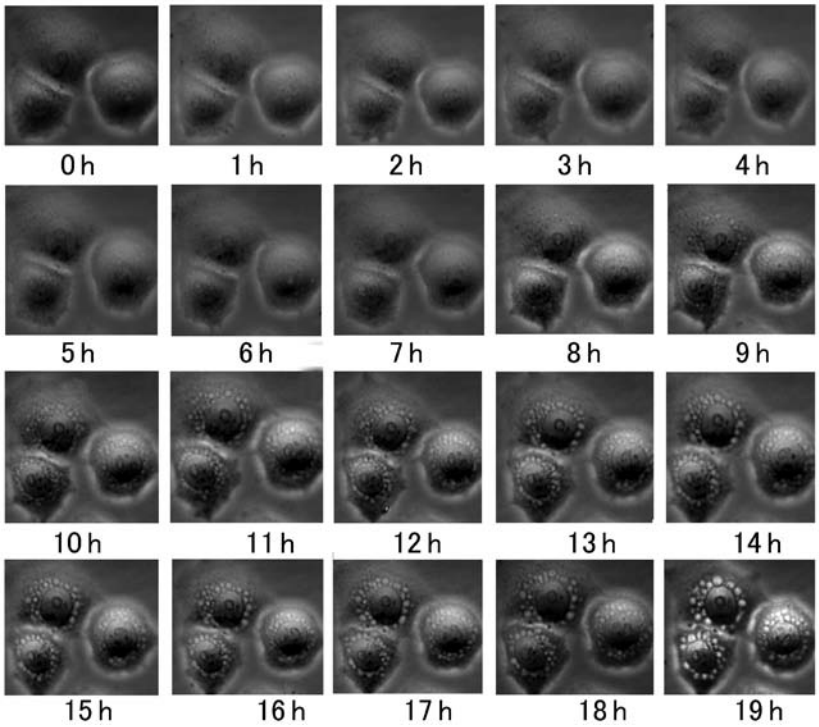

Figure 2. RHL induces vacuolar degeneration in HeLa cells in a time-dependent manner. HeLa cells in the logarithmic growth phase were treated with 160 μmol/l RHL and the cell morphology (magnification, x40) was recorded using a live cell-imaging system every 5 min for 24 h. A total of 20 images were selected to show the process of vacuole formation. RHL, Rhein lysinate.

Western blotting. HeLa cells were grown to 90% confluence in 25 cm^2 flasks in DMEM supplemented with 10% FBS, 100 μg/ml of streptomycin and 100 U/ml of penicillin. Cells were subsequently incubated for 12 h in DMEM supplemented with 0.1% FBS. The cells were treated with 160 μmol/l RHL for 0, 24, 48 and 72 h. Cells were scraped, and pellets were lysed using RIPA lysis buffer containing 150 mmol/l NaCl, 1% NP-40, 0.5% deoxycholate, 0.1% SDS and 50 mmol/l Tris-HCl (pH 7.4) (Roche Diagnostics, Basel, Switzerland) and lysed on ice for 15 min. Following centrifugation at 22,000 x g for 4 min at 4˚C, proteins in the supernatant were quantified using a protein assay (Bio-Rad Laboratories, Inc., Hercules, CA, USA). Samples were stored at -70˚C until analysis. Samples were mixed with an equal amount of Laemmli sample buffer (Bio-Rad Laboratories, Inc.) and boiled at 100˚C for 5 min. Isolated proteins (40 μg) were resolved on 10% SDS-PAGE and transferred to PVDF membranes using a semidry transfer apparatus (both from Bio-Rad Laboratories, Inc.). The membranes were incubated in blocking buffer [5% non-fat milk dissolved in TBS with 0.1% Tween-20 (TBST)] for 1 h at room temperature, followed by overnight incubation with primary antibodies at 4˚C. Subsequently, the membranes were incubated with the secondary antibody at room temperature for 2 h following washing three times with TBST. β-actin was used as the loading control. Protein bands were developed using Immobilon Western Chemiluminescent HRP substrate (cat. no. WBKLS0100; EMD Millipore) and images were captured using an enhanced ChemiImager 5500 chemiluminescence system (ProteinSimple, San Jose, CA, USA). ImageJ software (version 1.0; NIH) was used to quantify the optical density for treated samples, which were normalized to the β-actin internal controls.

Statistical analysis. Data are expressed as the mean ± standard deviation. The statistical analysis was conducted with one-way analysis of variance with the least significant difference post hoc test using IBM SPSS Statistics 19.0 software (IBM Corp., Armonk, NY, USA) and $P<0.05$ was considered to indicate a statistically significant difference.

Results

RHL inhibits HeLa cell proliferation. RHL inhibited HeLa cell proliferation in a dose-dependent manner (Fig. 1). In the present study, when HeLa cells were treated with 160 μmol/l RHL for 6 h, vacuoles were observed in the cytoplasm near the nucleus. The formation of vacuoles was recorded using a live cell-imaging system and increased in size over time (Fig. 2).

RHL-induced vacuoles in HeLa cells arise from mitochondria or endoplasmic reticulum. Transmission electron microscopy was performed to observe HeLa cells following treatment with 160 μmol/l for 24 h. Vacuoles had a complete membrane structure and some were also observed to have mitochondrial cristae, suggesting that they formed from endoplasmic reticulum or mitochondria damaged by RHL treatment. Mitochondrial cristae were observed in small vacuoles; however, they were not present in large vacuoles (Fig. 3).

Mitochondrial proteomic changes induced by RHL. Following treatment with 0, 80 or 160 μmol/l RHL for 24 h, mitochondria were extracted and a proteomic assay was performed by LC-MS/MS (Fig. 4). The results revealed that 138 genes were differentially expressed between treatment groups (0 vs. 80 μmol/l, 0 vs. 160 μmol/l and 80 vs. 160 μmol/l).

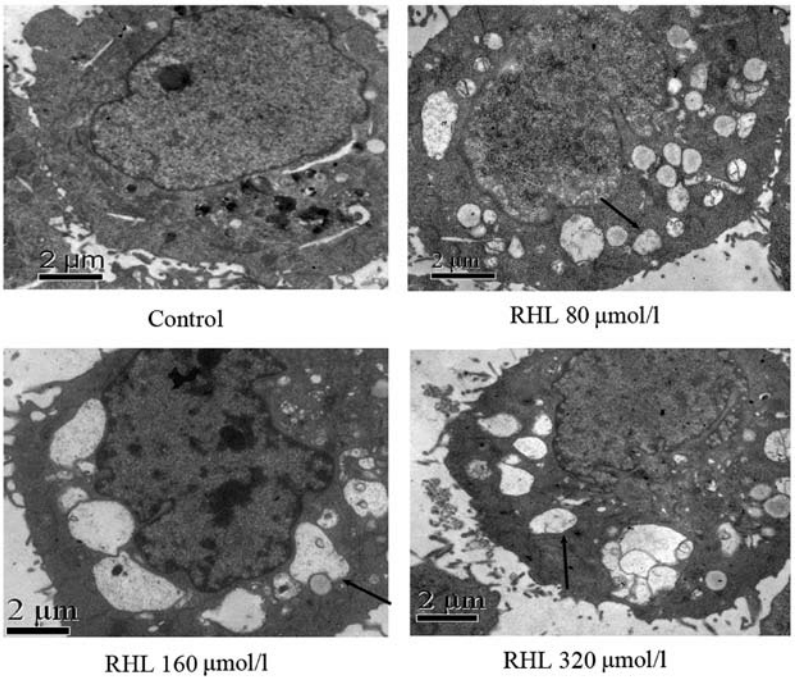

Figure 3. Vacuoles come from lesions of the endoplasmic reticulum and mitochondria. HeLa cells in the logarithmic growth phase were treated with 160 μmol/l RHL for 24 h and collected for transmission electron microscopy. Black arrows represent denatured mitochondria. RHL, Rhein lysinate.

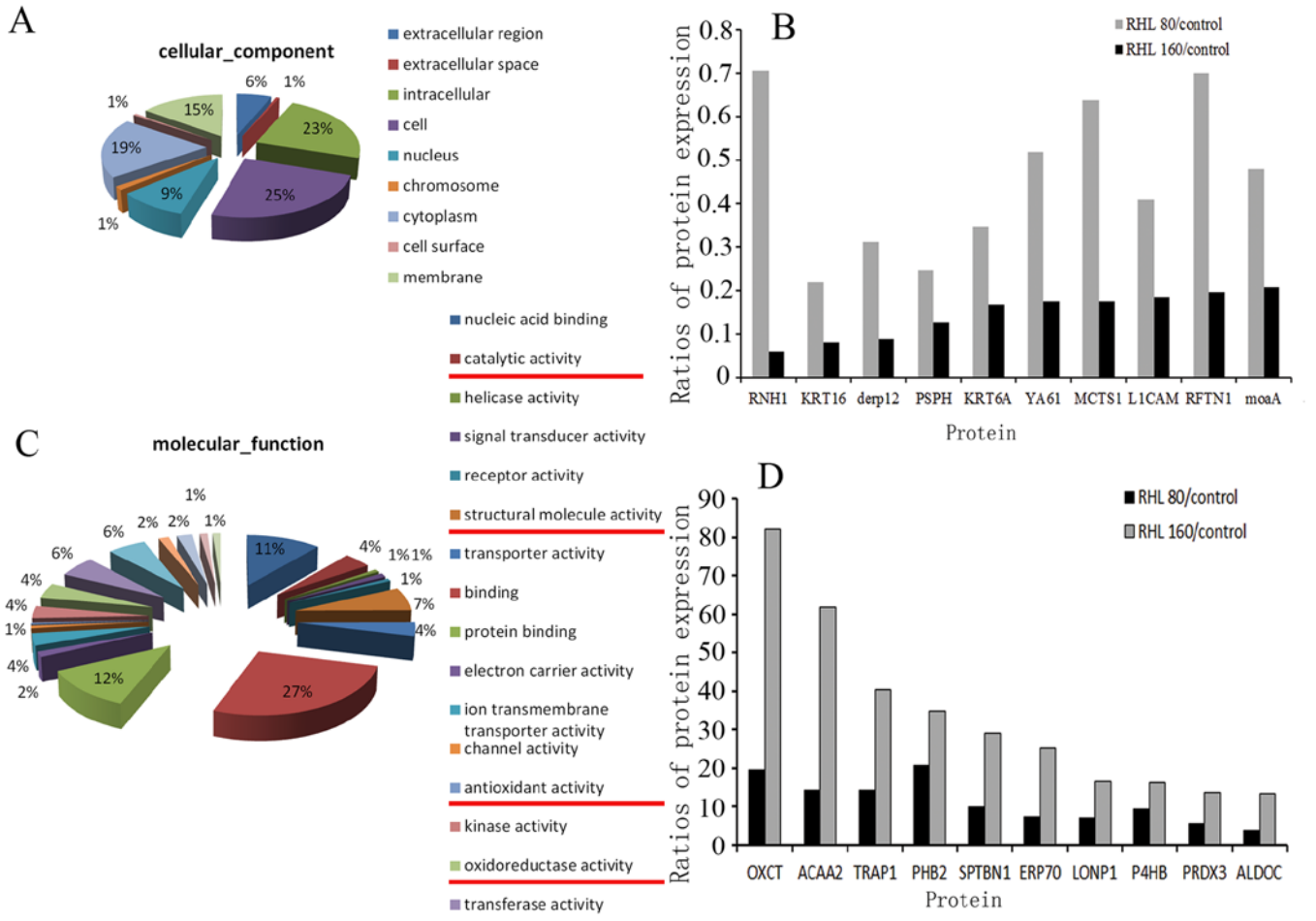

Figure 4. Vacuolar degeneration-associated mitochondrial proteomics changes. Changes in (A) cellular components following treatment with 160 μmol/l RHL. (B) Compared with untreated control group, the expression levels of RNH1, KRT16, derp12, PSPH, KRT6A, YA61, MCTS1, L1CAM, RFTN1 and moaA were decreased in cells treated with 80 or 160 μmol/l RHL. Changes in (C) molecular function following treatment with 160 μmol/l RHL. (D) Compared with control group, the expression levels of OXCT, ACAA2, TRAP1, PHB2, SPTBN1, ERP70, LONP1, P4HB, PRDX3 and ALDOC were increased in cells treated with 80 or 160 μmol/l RHL. RHL, Rhein lysinate.

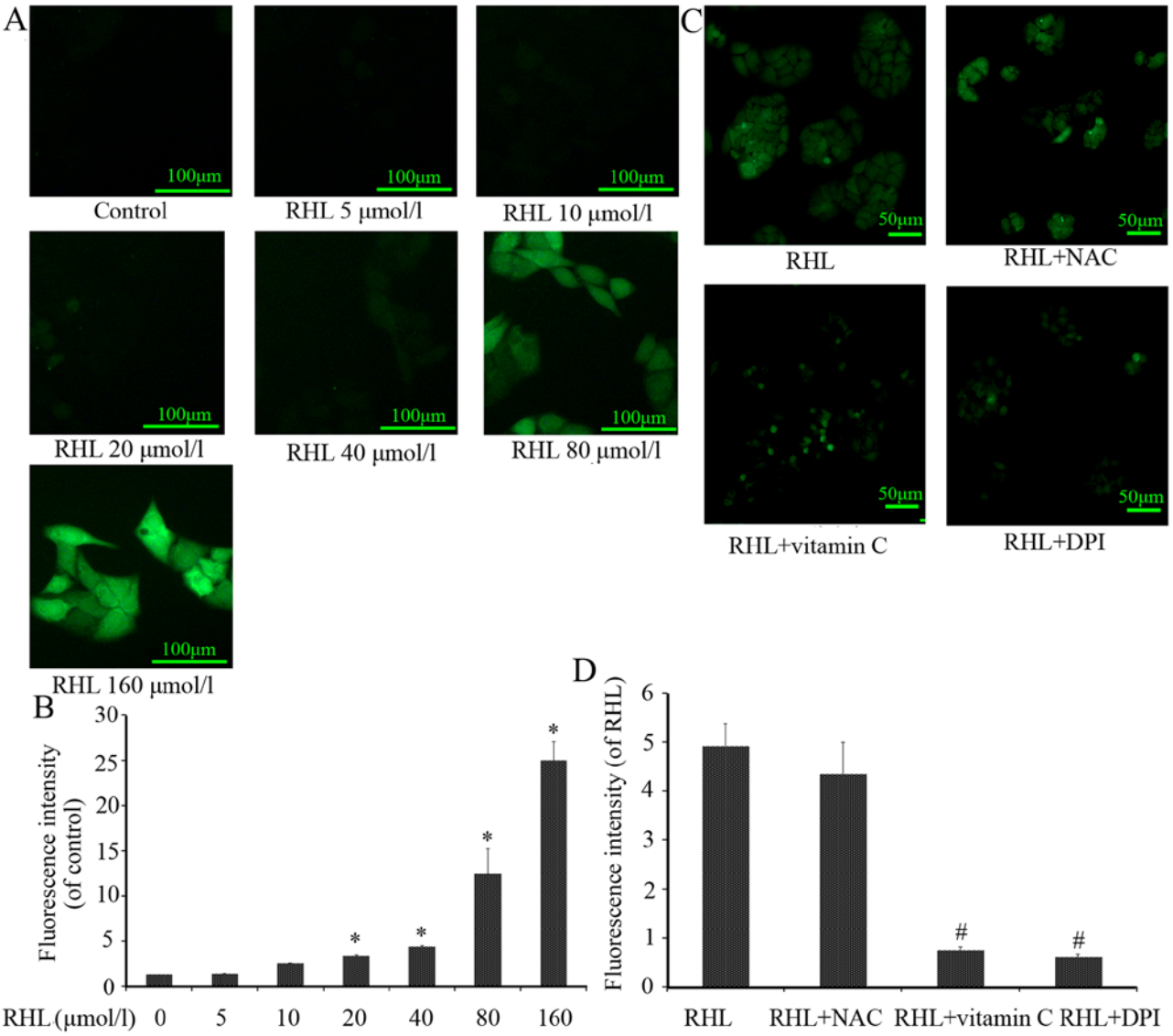

Figure 5. Effect of RHL on ROS. Intracellular ROS generation is an early event of RHL-induced cell apoptosis. (A) Representative images (magnification, x20) of the effects 0, 5, 10, 20, 40, 80 or 160 μmol/l RHL on intracellular ROS levels following 24-h treatment. (B) Representative images (magnification, x10) and quantification of HeLa cells treated with 160 μmol/l RHL, 160 μmol/l RHL+10 mmol/l NAC, 160 μmol/l RHL+10 mmol/l vitamin C, or 160 μmol/l RHL+5 μmol/l DPI for 24 h. Intracellular ROS levels were measured using fluorescence microscopy. (C) Quantification of (A). (D) Quantification of (B). *P<0.05, compared with the untreated control group; #P<0.05, compared with RHL group. ROS, reactive oxygen species; NAC, N-acetyl cysteine; DPI, diphenylene iodonium; RHL, Rhein lysinate.

Approximately 23% of these genes were associated with protein/nucleic acid binding, while others were associated with structural molecular activity, oxidoreductase activity, antioxidant activity and catalytic activity (Fig. 4A and C). Further analysis revealed that compared with control group, cytoskeletal protein keratin and dermal papilla derived protein 12 (DERP12), which is associated with the oxidation-reduction process, were most significantly decreased in the two RHL-treated groups. Both of which, are associated with mitochondrial structure and function. The top 10 upregulated and downregulated proteins are presented in Fig. 4B and D. In addition, the expression of proteins associated with cell proliferation, including Rac family small GTPase 1, signal transducer and activator of transcription 3, mitogen-activated protein kinase kinase 2, SMAD family member (SMAD)2 and SMAD4, were decreased following RHL treatment.

RHL increases ROS levels. ROS are primarily produced in the mitochondria by the oxidative respiratory chain. If mitochondria are damaged, their contents and function are affected. ROS levels were significantly increased following RHL treatment in a dose-dependent manner compared with the control group (Fig. 5). In addition, increased ROS levels following treatment with 160 μmol/l RHL were partly scavenged by vitamin C or DPI, whereas NAC exhibited no significant effect (Fig. 5).

RHL destroys mitochondrial membrane potential. MMP is a hallmark of mitochondrial function. To identify mitochondrial dysfunction induced by RHL, MMP was assessed following RHL treatment using Rhodamine 123 staining. Compared with the control group, treatment with 320 μmol/l RHL significantly inhibited Rhodamine 123 uptake in HeLa cells (Fig. 6).

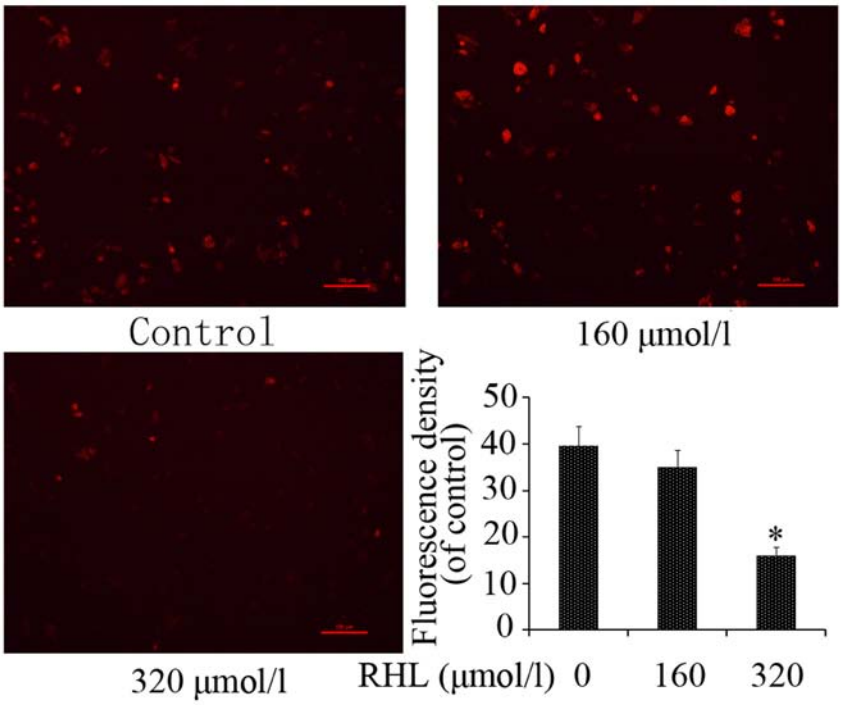

Figure 6. Changes in the MMP. Following treatment with various concentrations of RHL for 24 h, cells were stained with Rhodamine 123 and analyzed using fluorescence microscopy to evaluate the changes in MMP. Scale bar, 100 μm. *P<0.05, compared with control group. RHL, Rhein lysinate; MMP, mitochondrial membrane potential.

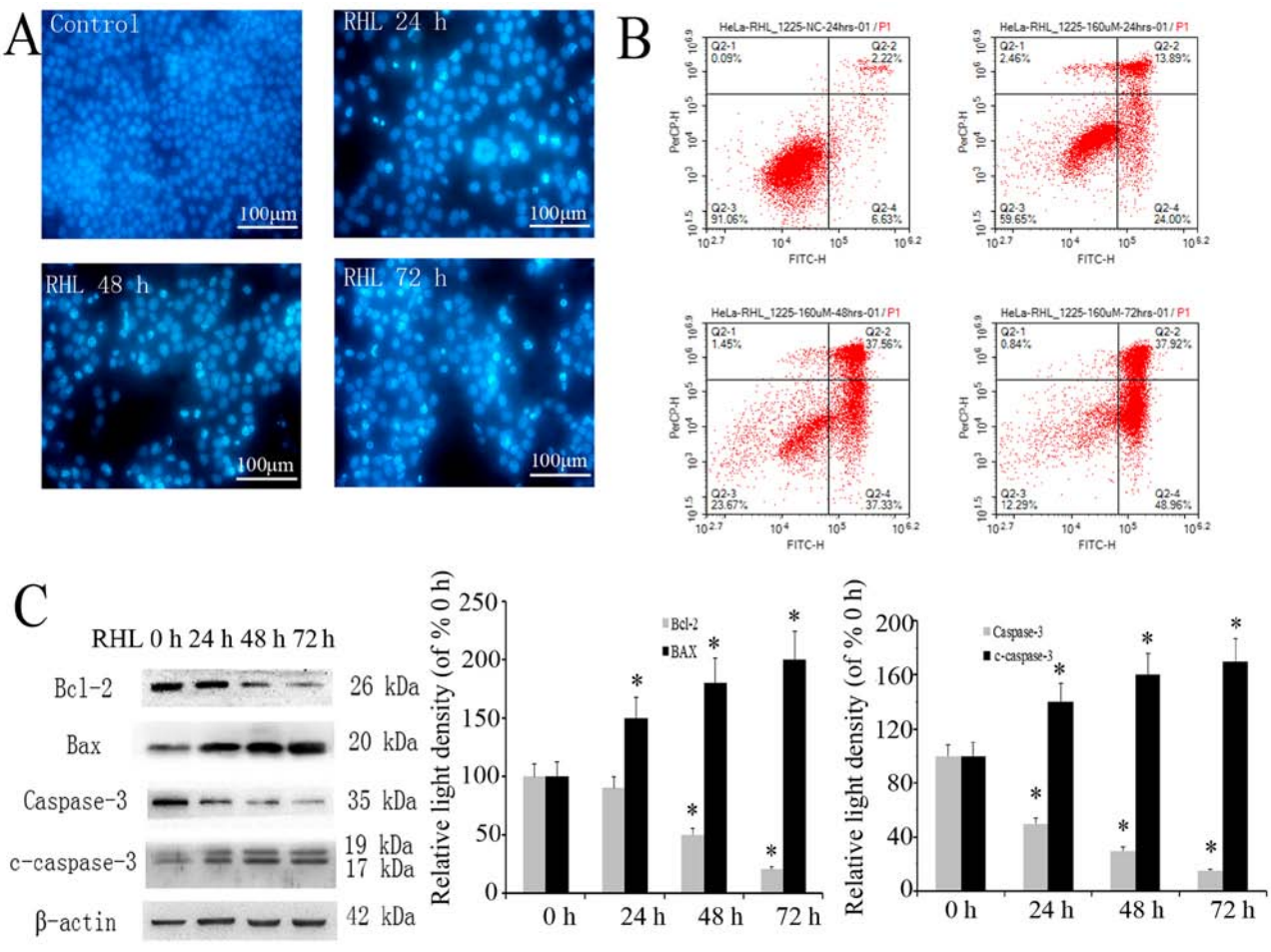

Figure 7. Effects of RHL on apoptosis. (A) Hoechst staining of HeLa cells following treatment with 160 μmol/l RHL for 24, 48 or 72 h. Apoptotic cells are stained bright turquoise (magnification, x20). (B) Cell apoptosis was detected using flow cytometry with Annexin V-PI stain. (C) Western blotting demonstrated that RHL treatment affects the expression of apoptosis-associated proteins. *P<0.05, compared with 0 h. PI, propidium iodide; RHL, Rhein lysinate.

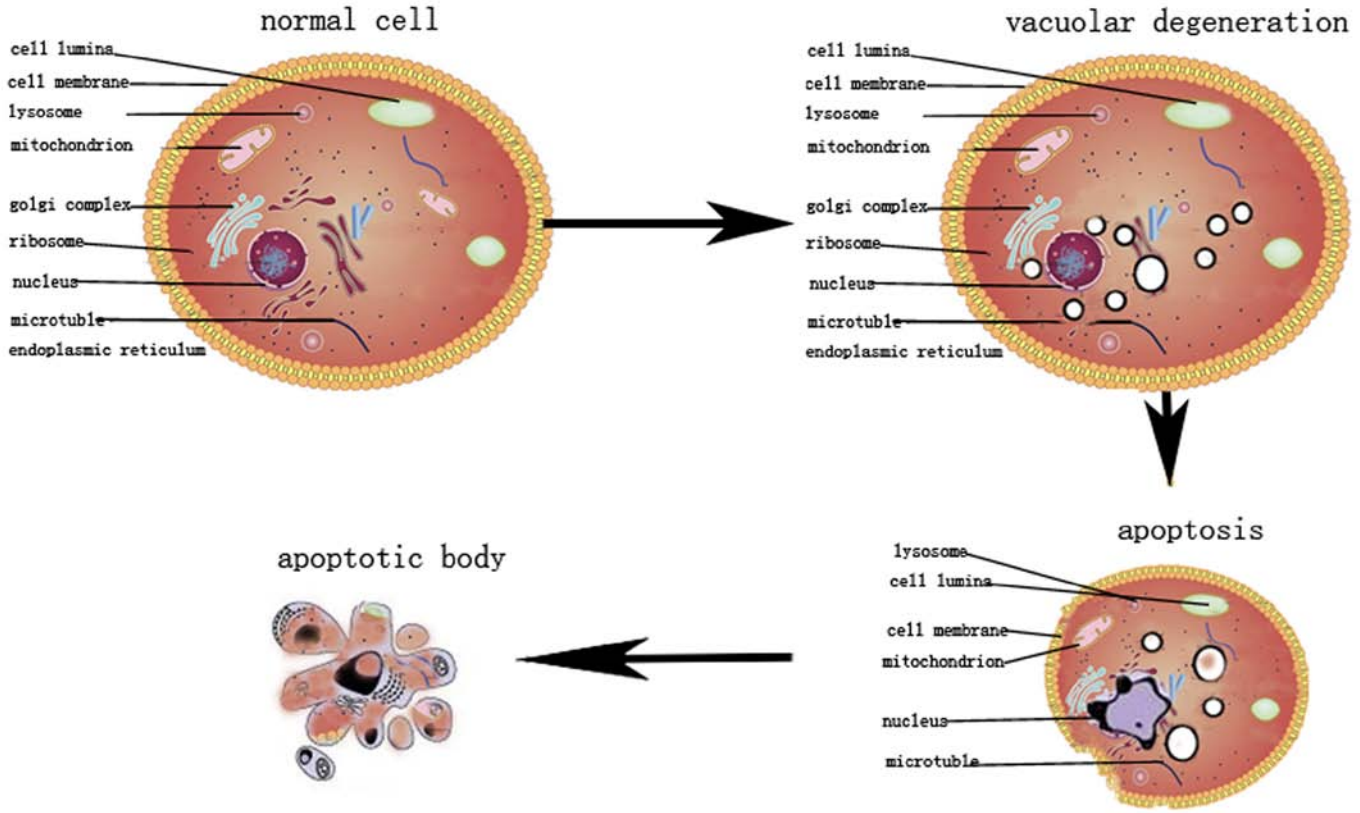

Figure 8. Signaling pathway of RHL-induced cell death. HeLa cells treated with 160 μmol/l RHL for 6 h developed vacuoles in the cytoplasm near the cell nucleus. The number and volume of vacuoles increased in a time-dependent manner and apoptosis was induced following 48 h RHL treatment. RHL, Rhein lysinate.

RHL induces mitochondrial pathway-dependent apoptosis. In the present study, short-term RHL treatment induced vacuolar degeneration in HeLa cells, while long-term RHL treatment induced cell death. To assess whether this is due to apoptosis, nuclear Hoechst and Annexin V/PI double-staining was performed. Compared with control group, the nuclear concentration, nucleus edge set and apoptotic body were observed in nucleus of HeLa cells treated with 160 μmol/l RHL by fluorescence microscope (Fig. 7A). Flow cytometry analysis revealed that the number of Annexin V-positive cells was increased by RHL treatment in a dose-dependent manner compared with control group (Fig. 7B). To evaluate the apoptosis-associated pathway, caspase-3, Bcl-2 and Bax expression was assessed using western blotting. As expected, RHL increased the cleavage of caspase-3, while Bax expression was significantly upregulated and Bcl-2 expression was downregulated (Fig. 7C). These results suggest that RHL induces apoptosis via regulating apoptosis-associated proteins.

Discussion

Mitochondria serve important roles in the regulation of a wide variety of intracellular processes, including providing a source of ATP energy, generating reactive oxygen species (18,19), and regulating intracellular Ca^{2+} homeostasis (20), iron-sulfur protein assembly (21,22), apoptosis (23-25) and mitophagy (26,27). During cell reprogramming and cellular transformation, mitochondria undergo dynamic changes (28). In the present study, mitochondrial dynamic changes were first observed when HeLa cells were treated with 160 μmol/l RHL. The earliest change in mitochondrial morphology, which appeared 6 h following treatment, was vacuolar degeneration. Rhein is a weakly acidic molecule. Therefore, it exists in two forms: Non-dissociation and dissociation. It is considered that the non-dissociation form of Rhein penetrates the cell membrane by active diffusion (29). When levels of the non-dissociation form of Rhein are reduced, the dissociation form of Rhein turns into the non-dissociation form. In the current study, Rhein lysinate was demonstrated to inhibit the expression of keratin 16 and keratin 6A in proteomics analysis. It was reported that keratin 16 was a type I cytokeratin and was paired with keratin 6 in a number of epithelial tissues (30). Type I keratins (or Type I cytokeratins) are cytokeratins that constitute the Type I intermediate filaments of the intracytoplasmatic cytoskeleton (31). Thus, it is considered that vacuolar degeneration of mitochondrion is induced by the destruction of the cytoskeleton.

Apoptosis is characterized by cell shrinkage, blebbing of the plasma membrane, maintenance of organelle integrity, condensation and fragmentation of DNA, followed by ordered removal of phagocytes to minimize damage to surrounding tissues (32). Apoptosis has been classified into two types depending on the mechanistic pathway responsible, namely the extrinsic pathway and the mitochondria-mediated pathway (33,34). Following treatment with 160 μmol/l RHL for 24, 48 or 72 h, HeLa cell apoptosis was observed using flow cytometry. Bcl-2 is a prototypical anti-apoptotic member of the Bcl-2 family (35), while Bax is pro-apoptotic (36). Bax

is a functional antagonist of Bcl-2, and the Bcl-2/Bax ratio regulates cell apoptosis (35,37,38). In the present study, RHL treatment was demonstrated to decrease Bcl-2 expression and increase Bax expression, thereby reducing the Bcl-2/Bax ratio in HeLa cells.

A number of studies have reported that ROS serves an important role in carcinogenesis. For example, at low physiological concentrations ROS regulate cell growth; however, at high concentrations, ROS serves a role in oxidative stress and the induction of apoptosis (39-41). Non-thermal plasma induces the mitochondria-mediated apoptotic signaling pathway via ROS generation in HeLa cells (42). In the present study, it was revealed that RHL induces ROS generation in HeLa cells in dose-dependent manner. Antioxidants, including vitamin C and DPI, are able to partially inhibit RHL-induced ROS generation. In addition, the antioxidant activity of certain genes, such as DERP12, may decrease and others, such as PRDX3, may increase, as indicated by in proteomics analysis. As a whole, the ROS level of mitochondrion was increased. It may be deduced that ROS participates in the process by which RHL induces HeLa cell apoptosis.

It should be noted that there are a number of fluorescent mitochondrial dyes that may be used for MMP measurements (43). Different probes are recommended for each usage paradigm, depending on the uptake kinetics, concentration and mitochondrial binding affinity of the probe (44). Rhodamine 123 is recommended for applications that aim to measure rapid changes in membrane potential (45,46). In the present study, 320 μmol/l RHL was revealed to decrease the MMP of HeLa cells. However, the mechanism of RHL decreasing MMP is unclear and requires further study.

In conclusion, RHL exhibits a dynamic influence on HeLa cells, causing vacuolar degeneration after 6 h and apoptosis after 24 h of treatment (Fig. 8). It was hypothesized that the vacuolar degeneration and apoptosis-associated signal pathways may be an appealing target for therapeutic interventions in cervical carcinoma. Future studies should investigate the antitumor effect of RHL in patients with cervical cancer.

Acknowledgements

Not applicable.

Funding

The present study was supported by grants from the National Natural Science Foundation of China (grant no. 81671391) and the Beijing Hospital Nova project (grant no. BJ-2016-033).

Availability of data and materials

The datasets used and/or analyzed during the current study are available from the corresponding author on reasonable request.

Authors' contributions

YL and PT conceived and designed the experiments; JL, YZ and JC performed the experiments; YL and RX analyzed the data; JW assisted in flow cytometric analysis and manuscript preparation; GH assisted in western blot analysis and manuscript preparation; YL wrote the manuscript.

Ethics approval and consent to participate

Not applicable.

Patient consent for publication

Not applicable.

Competing interests

The authors declare that they have no competing interests.

References

1. Waggoner SE: Cervical cancer. Lancet 361: 2217-2225, 2003.
2. Peralta-Zaragoza O, Bermúdez-Morales VH, Pérez-Plasencia C, Salazar-León J, Gómez-Cerón C and Madrid-Marina V: Targeted treatments for cervical cancer: A review. OncoTargets Ther 5: 315-328, 2012.
3. He AD, Wang SP, Xie W, Song W, Miao S, Yang RP, Zhu Y, Xiang JZ and Ming ZY: Platelet derived TGF-β promotes cervical carcinoma cell growth by suppressing KLF6 expression. Oncotarget 8: 87174-87181, 2017.
4. Shimizu K, Kageyama M, Ogura H, Yamada T and Shimazu T: Effects of Rhubarb on intestinal dysmotility in critically ill patients. Intern Med 57: 507-510, 2018.
5. Gao D, Zeng LN, Zhang P, Ma ZJ, Li RS, Zhao YL, Zhang YM, Guo YM, Niu M, Bai ZF, *et al*: Rhubarb anthraquinones protect Rats against Mercuric Chloride ($HgCl_2$)-induced acute renal failure. Molecules 21: 298, 2016.
6. Neyrinck AM, Etxeberria U, Taminiau B, Daube G, Van Hul M, Everard A, Cani PD, Bindels LB and Delzenne NM: Rhubarb extract prevents hepatic inflammation induced by acute alcohol intake, an effect related to the modulation of the gut microbiota. Mol Nutr Food Res 61: 61, 2017.
7. Huang Q, Lu G, Shen HM, Chung MC and Ong CN: Anti-cancer properties of anthraquinones from rhubarb. Med Res Rev 27: 609-630, 2007.
8. Morrison DK: MAP kinase pathways. Cold Spring Harb Perspect Biol 4: 4, 2012.
9. Hsia TC, Yang JS, Chen GW, Chiu TH, Lu HF, Yang MD, Yu FS, Liu KC, Lai KC, Lin CC, *et al*: The roles of endoplasmic reticulum stress and Ca^{2+} on rhein-induced apoptosis in A-549 human lung cancer cells. Anticancer Res 29: 309-318, 2009.
10. Heo SK, Yun HJ, Park WH and Park SD: Rhein inhibits TNF-alpha-induced human aortic smooth muscle cell proliferation via mitochondrial-dependent apoptosis. J Vasc Res 46: 375-386, 2009.
11. Sun H, Luo G, Chen D and Xiang Z: A comprehensive and system review for the pharmacological mechanism of action of rhein, an active anthraquinone ingredient. Front Pharmacol 7: 247, 2016.
12. Lin YJ and Zhen YS: Rhein lysinate suppresses the growth of breast cancer cells and potentiates the inhibitory effect of Taxol in athymic mice. Anticancer Drugs 20: 65-72, 2009.
13. Liu J, Zhang K, Zhen YZ, Wei J, Hu G, Gao JL, Tian YX and Lin YJ: Antitumor activity of rhein lysinate against human glioma U87 cells in vitro and in vivo. Oncol Rep 35: 1711-1717, 2016.
14. Lin YJ, Zhen YZ, Zhao YF, Wei J and Hu G: Rhein lysinate induced S-phase arrest and increased the anti-tumor activity of 5-FU in HeLa cells. Am J Chin Med 39: 817-825, 2011.
15. Zhen YZ, Hu G, Zhao YF, Yan F, Li R, Gao JL and Lin YJ: Synergy of Taxol and rhein lysinate associated with the down-regulation of ERK activation in lung carcinoma cells. Oncol Lett 6: 525-528, 2013.
16. Paglin S, Hollister T, Delohery T, Hackett N, McMahill M, Sphicas E, Domingo D and Yahalom J: A novel response of cancer cells to radiation involves autophagy and formation of acidic vesicles. Cancer Res 61: 439-444, 2001.

17. Dzieciatkowska M, Qi G, You J, Bemis KG, Sahm H, Lederman HM, Crawford TO, Gelbert LM, Rothblum-Oviatt C and Wang M: Proteomic characterization of cerebrospinal fluid from ataxia-telangiectasia (A-T) patients using a LC/MS-based label-free protein quantification technology. Int J Proteomics 2011: 578903, 2011.
18. Faulk A, Weissig V and Elbayoumi T: Mitochondria-specific nano-emulsified therapy for myocardial protection against doxorubicin-induced cardiotoxicity. Methods Mol Biol 991: 99-112, 2013.
19. Pohjoismäki JL and Goffart S: The role of mitochondria in cardiac development and protection. Free Radic Biol Med 106: 345-354, 2017.
20. Park SJ, Lee SB, Suh Y, Kim SJ, Lee N, Hong JH, Park C, Woo Y, Ishizuka K, Kim JH, *et al*: DISC1 modulates neuronal stress responses by gate-keeping ER-mitochondria Ca^{2+}transfer through the MAM. Cell Reports 21: 2748-2759, 2017.
21. Wachnowsky C, Fidai I and Cowan JA: Iron-sulfur cluster biosynthesis and trafficking - impact on human disease conditions. Metallomics 10: 9-29, 2018.
22. Stehling O, Wilbrecht C and Lill R: Mitochondrial iron-sulfur protein biogenesis and human disease. Biochimie 100: 61-77, 2014.
23. Burke PJ: Mitochondria, bioenergetics and apoptosis in cancer. Trends Cancer 3: 857-870, 2017.
24. Duan H, Wang R, Yan X, Liu H, Zhang Y, Mu D, Han J and Li X: Phloretin induces apoptosis of human esophageal cancer via a mitochondria-dependent pathway. Oncol Lett 14: 6763-6768, 2017.
25. Park S, Lim W, Bazer FW and Song G: Naringenin induces mitochondria-mediated apoptosis and endoplasmic reticulum stress by regulating MAPK and AKT signal transduction pathways in endometriosis cells. Mol Hum Reprod 23: 842-854, 2017.
26. Ułamek-Kozioł M, Kocki J, Bogucka-Kocka A, Januszewski S, Bogucki J, Czuczwar SJ and Pluta R: Autophagy, mitophagy and apoptotic gene changes in the hippocampal CA1 area in a rat ischemic model of Alzheimer's disease. Pharmacol Rep 69: 1289-1294, 2017.
27. Rodger CE, McWilliams TG and Ganley IG: Mammalian mitophagy - from in vitro molecules to in vivo models. FEBS J 285: 1185-1202, 2018.
28. Prieto J and Torres J: Mitochondrial dynamics: In cell reprogramming as it is in cancer. Stem Cells Int 2017: 8073721, 2017.
29. Peng Y, Fan M, Peng C, Wang M and Li X: Alleviating the intestinal absorption of rhein in Rhubarb through herb compatibility in Tiaowei Chengqi Tang in Caco-2 cells. Evid Based Complement Alternat Med 2018:7835128. eCollection 2018.
30. Trost A, Desch P, Wally V, Haim M, Maier RH, Reitsamer HA, Hintner H, Bauer JW and Onder K: Aberrant heterodimerization of keratin 16 with keratin 6A in HaCaT keratinocytes results in diminished cellular migration. Mech Ageing Dev 131: 346-353, 2010.
31. Herrmann H, Bär H, Kreplak L, Strelkov SV and Aebi U; Herrmann H1: Bär H, Kreplak L, Strelkov SV and Aebi U. Intermediate filaments: From cell architecture to nanomechanics. Nat Rev Mol Cell Biol 8: 562-573, 2007.
32. Brenner C and Kroemer G: Apoptosis. Mitochondria - the death signal integrators. Science 289: 1150-1151, 2000.
33. Low IC, Kang J and Pervaiz S: Bcl-2: A prime regulator of mitochondrial redox metabolism in cancer cells. Antioxid Redox Signal 15: 2975-2987, 2011.
34. Indran IR, Tufo G, Pervaiz S and Brenner C: Recent advances in apoptosis, mitochondria and drug resistance in cancer cells. Biochim Biophys Acta 1807: 735-745, 2011.
35. Vucicevic K, Jakovljevic V, Colovic N, Tosic N, Kostic T, Glumac I, Pavlovic S, Karan-Djurasevic T and Colovic M: Association of Bax expression and Bcl2/Bax ratio with clinical and molecular prognostic markers in chronic lymphocytic leukemia. J Med Biochem 35: 150-157, 2016.
36. Pawlowski J and Kraft AS: Bax-induced apoptotic cell death. Proc Natl Acad Sci USA 97: 529-531, 2000.
37. Siqueira EC, Souza FT, Diniz MG, Gomez RS and Gomes CC: Hsp27 (HSPB1) differential expression in normal salivary glands and pleomorphic adenomas and association with an increased Bcl2/Bax ratio. Tumour Biol 36: 213-217, 2015.
38. Muhammad Nadzri N, Abdul AB, Sukari MA, Abdelwahab SI, Eid EE, Mohan S, Kamalidehghan B, Anasamy T, Ng KB, Syam S, *et al*: Inclusion complex of Zerumbone with hydroxypropyl- β -cyclodextrin induces apoptosis in liver hepatocellular HepG2 cells via caspase 8/BID cleavage switch and modulating Bcl2/Bax ratio. Evid Based Complement Alternat Med 2013: 810632, 2013.
39. Fakhri A, Omranipour R, Fakhri S, Mirshamsi M, Zangeneh F, Vatanpour H and Pourahmad J: *Naja naja* oxiana venom fraction selectively induces ROS-mediated apoptosis in human colorectal tumor cells by directly targeting mitochondria. Asian Pac J Cancer Prev 18: 2201-2208, 2017.
40. Pant K, Yadav AK, Gupta P, Islam R, Saraya A and Venugopal SK: Butyrate induces ROS-mediated apoptosis by modulating miR-22/SIRT-1 pathway in hepatic cancer cells. Redox Biol 12: 340-349, 2017.
41. Alarifi S, Ali D, Alkahtani S and Almeer RS: ROS-mediated apoptosis and genotoxicity induced by palladium nanoparticles in human skin malignant melanoma cells. Oxid Med Cell Longev 2017: 8439098, 2017.
42. Li W, Yu KN, Ma J, Shen J, Cheng C, Zhou F, Cai Z and Han W: Non-thermal plasma induces mitochondria-mediated apoptotic signaling pathway via ROS generation in HeLa cells. Arch Biochem Biophys 633: 68-77, 2017.
43. Perry SW, Norman JP, Barbieri J, Brown EB and Gelbard HA: Mitochondrial membrane potential probes and the proton gradient: A practical usage guide. Biotechniques 50: 98-115, 2011.
44. Zhu C, Martinez AF, Martin HL, Li M, Crouch BT, Carlson DA, Haystead TAJ and Ramanujam N: Near-simultaneous intravital microscopy of glucose uptake and mitochondrial membrane potential, key endpoints that reflect major metabolic axes in cancer. Sci Rep 7: 13772, 2017.
45. Sun LL, Sun LR and Wang GY: Mitochondrial membrane potential at HL-60 cell apoptosis induced by cytarabine. Zhongguo Shi Yan Xue Ye Xue Za Zhi 15: 1196-1199, 2007 (In Chinese).
46. Peatey CL, Chavchich M, Chen N, Gresty KJ, Gray KA, Gatton ML, Waters NC and Cheng Q: Mitochondrial membrane potential in a small subset of artemisinin-induced dormant *Plasmodium falciparum* parasites in vitro. J Infect Dis 212: 426-434, 2015.